Improving the efficiency of liver targeting rAAV-mediated homologous recombination using ribonucleotide reductase inhibitors

Shinnosuke Tsuji
Stanford Univ
Calvin Stevens
Stanford UNiv
Giulia Bortolussi
Univ Trieste
Feijie Zhang
Stanford University School of Medicine
Katja Pekrun
Stanford Univ https://orcid.org/0000-0001-8346-1889
Gabriele Baj
Univ Trieste
Gustavo de Alencastro
Stanford University
Andres Muro
International Centre for Genetic Engineering and Biotechnology (ICGEB) https://orcid.org/0000-0002-9628-0494
Mark Kay (markay@stanford.edu)
Stanford University https://orcid.org/0000-0002-2799-2615

Article

Keywords: Therapeutic Gene Delivery, Transgene Expression, Fludarabine, Non-proliferating Hepatocytes, Transient DNA Repair Signaling

Posted Date: December 10th, 2020

DOI: https://doi.org/10.21203/rs.3.rs-106148/v1

Version of Record: A version of this preprint was published at Nature Biotechnology on April 7th, 2022. See the published version at https://doi.org/10.1038/s41587-022-01240-2.

Abstract

Recombinant adeno-associated viral (rAAV) vectors continue to gain popularity for *in vivo* therapeutic gene delivery. Homologous recombination-based gene therapy using rAAV (AAV-HR) without nucleases has several advantages over classical gene therapy, especially when targeting the liver in neonatal/pediatric populations due to its potential for permanent sustained transgene expression. However, the low efficiency of AAV-HR remains a limitation for some clinical applications. Here, we tested series of small molecule compounds with different mechanisms of action in the context of AAV-HR and identified that ribonucleotide reductase (RNR) inhibitors significantly enhanced the AAV-HR efficiency in mouse and human liver cell lines. Furthermore, short term administration of the RNR inhibitor fludarabine increased the *in vivo* efficiency of both non-nuclease and CRISPR/Cas9-mediated AAV-HR in the murine liver, without causing toxicity. Mechanistic experiments showed that fludarabine administration induced transient DNA damage signaling in both proliferating and quiescent hepatocytes. Surprisingly, *in vivo* BrdU labeling implicated that the majority of AAV-HR events occurred in non-proliferating hepatocytes in both fludarabine-treated and control mice. These studies suggested that the induction of transient DNA repair signaling in non-dividing hepatocytes was responsible for enhancing the efficiency of AAV-HR in mice during RNR inhibition. In total, we show the use of a clinically approved RNR inhibitor can enhance AAV-HR based genome editing therapeutics.

Introduction

Recombinant adeno-associated virus (rAAV) are increasingly popular vectors for gene transfer having achieved recent FDA approval of several rAAV-based gene therapies[1,2]. Although the liver is an attractive target organ for rAAV gene therapy, it is clear that classical gene replacement approaches are unlikely to be applicable to newborn or pediatric patients. Hepatocyte proliferation and/or turnover results in loss of therapeutic expression from vector episomes[3–5].

As an alternative to gene replacement, we have developed a rAAV-based promotorless gene targeting strategy referred to as AAV-HR or GeneRide™ [6]. This gene editing technology targets the 3’ coding region of a highly expressed gene, such as *Albumin* (*Alb*), using homology arms surrounding a self-cleaving peptide (P2A) and a transgene. In this context, successful gene targeting via homologous recombination (HR) results in conversion of the native mRNA to a fusion mRNA (Alb-P2A-transgene) and translation of the endogenous and transgene proteins. This technology has shown permanent correction of several disease models[6,7].

Despite the effectiveness as a therapy, the overall rate of AAV-HR remains low. Furthermore, the molecular mechanism of the gene targeting is not fully understood. Here, we identify a small molecule drug that can be administered transiently and safely in combination with rAAV to enhance gene editing in somatic mammalian tissue.

Results

Inhibition of ribonuclease reductase enhanced gene targeting in cultured cells

To identify compounds that enhance AAV-HR, we evaluated the following small molecules reported to increase rAAV transduction: mTOR inhibitor (Torin-1), proteasome inhibitor (MG132), HDAC inhibitors (Trichostatin A, FK228), topoisomerase inhibitor (Teniposide), and a ribonucleotide reductase (RNR) inhibitor (Hydroxyurea)[8–16]. First, we treated a human hepatoma cell line, Huh7, with the above compounds and an AAV-DJ vector expressing luciferase[17]. As reported prior, all compounds significantly increased rAAV transduction measured by luciferase activity (Extended Fig.1a).

We next used a promoterless vector targeting the *Glyceraldehyde-3-Phosphate Dehydrogenase* (*GAPDH*) locus for HR, designated GAPDH-P2A-GFP, to evaluate AAV-HR efficiency. This vector allows for GFP expression only following HR at the target locus, allowing flow cytometry quantification of HR events (Fig.1a). As GAPDH-P2A-GFP lacks a promoter and start codon at the N-terminus of GFP, there is little functional expression from episomal rAAV genomes. When treated with hydroxyurea (HU), cells showed a 3 to 4-fold increase in GFP+ cells (Fig1.b) whereas most of other compounds failed to increase the GFP+ fraction (Extended Fig.1b).

A well-defined molecular target of HU is the RNR enzyme which generates deoxyribonucleotides from ribonucleotides[18]. Therefore, we examined other RNR inhibitors (fludarabine, triapine, gallium nitrate) and found these drugs also significantly enhanced transduction of rAAV, except gallium nitrate (Fig.1c)[18]. In the flow cytometry gene targeting assay, we observed an increase in GFP+ Huh7 cells pre-treated with fludarabine and triapine (Fig.1b). To validate RNR inhibition as the mechanism for increased gene targeting, we used siRNA knockdown of RRM1, the main subunit of the RNR complex[18]. Knockdown of RRM1 also increased GFP+ fractions in GAPDH-P2A-GFP transduced cells (Fig.1d-e). These data supported that suppression of RNR can enhance the efficiency of gene targeting *in vitro*.

To confirm on-target HR, we amplified genomic DNA at the left integration junction in Huh7 cells post-infection, using a primer binding to the upstream genomic sequence, past the homology arms, and a primer binding to the P2A sequence (Fig.1a). As such, correctly integrated genomic sequences with the expected size were amplified only in transduced cells (Fig.1f).

We next examined these compounds in the mouse hepatoma cell line Hepa1-6, using a vector targeting the mouse *Albumin* locus, named Alb-P2A-GFP (Fig.1g). Consistent with Huh7 data, HU or fludarabine pretreatment, prior to Alb-P2A-GFP infection, increased the GFP+ fractions in Hepa1-6 cells compared to controls (Fig.1g). To confirm targeted integration, we analyzed Albumin-P2A-GFP fusion mRNA levels by qPCR (Fig.1h). qPCR of fusion Albumin-P2A-GFP mRNA showed increased abundance in HU (3.5-fold) and fludarabine (2.6-fold) treated cells (Fig.1i). Taken together, the above data show RNR inhibitors increased the efficiency of AAV gene targeting *in vitro*, independent of species and target locus.

Fludarabine administration increased AAV-mediated gene targeting *in vivo*

To test RNR inhibitors *in vivo*, we injected the rAAV8-Alb-P2A-hF9 gene targeting vector**,** containing human *coagulation factor 9* (hF9) with homology arm targeting the mouse *Albumin* locus, with or without administration of HU or fludarabine (Fig.2a)[6]. Strikingly, we observed a sustained 2.7 to 4.6-fold increase of plasma hF9 levels in mice treated with fludarabine, but not HU, compared to control mice (Fig. 2b). We speculated the lack of efficacy in HU-treated mice might be due to its rapid liver metabolism[19]. Importantly, fludarabine administration did not delay body weight gain compared with PBS controls (Extended Fig.2a). In addition, no severe or irreversible toxicity was observed in fludarabine-injected mice based on complete blood counts, blood biochemical examination, and liver histopathological analysis by a trained veterinarian pathologist (Extended Fig.2b, Extended Fig.3, and Table 2). The copy number of rAAV genomes per diploid hepatocytes was similar between groups, regardless of drug treatment, showing increased hF9 expression was not the result of higher vector delivery into the liver (Fig.2c).

To confirm HR, we amplified the right-sided integration junction using a genomic-binding primer outside the homology arm (primer Rv) and a primer in *hF9* (primer Fw1) (Extended Fig.4a). We observed the on-target HR-derived amplicon at the expected size of 1.6 kb only in rAAV-injected mouse samples (Extended Fig.4b). A nested PCR showed a single band of expected size (1.5 kb) (primers Fw3 and Rv2), which was TOPO-cloned and 5 clones (one from each mouse) were Sanger sequenced, confirming correct on-target integration without any indels (Extended Fig.4c-d). We next quantified the amount of fusion hF9 mRNA derived from on-target integration (Fig.2d). Fusion mRNA levels were significantly higher in the fludarabine-treated versus control animals (5.1-fold increase) (Fig.2e). qPCR of total hF9 mRNA with vector-internal primers, which includes fusion mRNA from targeted integration, random integration, or episomal-derived expression, showed a 4.4-fold increase in fludarabine-treated versus control mice (Fig.2f). Endogenous albumin expression remained unchanged by fludarabine treatment (Fig.2g).

To obtain mRNA characteristics in mouse livers on a single cell level, we used RNAScope *in situ* hybridization to label hF9 and mAlb mRNAs following rAAV and fludarabine treatment. Endogenous mAlb mRNA was immensely abundant in all hepatocytes, while hF9 mRNA was expressed in relatively few hepatocytes (Fig.2h and Extended Fig.5). These infrequent hF9 mRNA positive cells were consistent with the low frequency of gene targeting[7,20]. hF9 mRNA positive cells displaying strong intracellular staining were more abundant in fludarabine versus PBS-treated animals. Collectively, the above data demonstrated that fludarabine increased hF9 expression through enhanced AAV-HR efficiency.

Next, we examined a fludarabine dose response. Five days of fludarabine treatment resulted in the highest plasma hF9 levels (6.4-fold vs. PBS) while even a single administration showed a 2-fold increase over controls (Fig2.i and Extended Fig.6a). We observed no significant decrease in body weight with longer fludarabine treatment (Extended Fig.6b). Furthermore, delayed fludarabine administration, four weeks after vector injection, did not enhance hF9 expression, suggesting that the effect of fludarabine on gene targeting requires proximity to the timing of rAAV transduction (Extended Fig.7). Lastly, fludarabine also enhanced gene targeting to the *ApoE* locus, demonstrating its effect is not restricted to *Alb* in mouse livers (Extended Fig.9).

To fully define the effect of fludarabine on liver transduction, we injected rAAV8-HLP-hAAT expressing human alpha-1-antitrypsin (hAAT) from the liver-specific HLP promoter, with or without fludarabine. Fludarabine transiently increased hAAT mRNA and serum levels 2-fold at three days post rAAV injection but returned to the same level as the controls eight days post-injection, remaining similar to controls for 11-weeks (Extended Fig.10). Furthermore, at 11-weeks, there were no differences in hAAT mRNA levels (Extended Fig.10). Furthermore, we determined neither HU nor fludarabine changed the amount of total nuclear or double-stranded rAAV genomes in Huh7 cells (Extended Fig.11). Overall, fludarabine may transiently affect rAAV-mediated transgene expression without altering nuclear entry, similar to reports using hydroxyurea *in vitro*[10].

Fludarabine transiently suppressed hepatocyte proliferation

RNR inhibitors (e.g. HU) are used to induce cell cycle arrest and synchronize cultured cells in S-phase; moreover, canonical HR is most active in the S/G2 phase of the cell cycle[21–24]. As such, we investigated the proliferation status of liver cells by measuring DNA synthesis via bromodeoxyuridine (BrdU) labeling. Mice were injected with BrdU for three days, with or without fludarabine, and liver sections were stained with an anti-BrdU antibody (Fig.3a and Extended Fig.12a-b). BrdU incorporation averaged ~50 positive nuclei per field of view in control mice, while BrdU labeled nuclei were nearly absent in fludarabine-treated mice, demonstrating a strong inhibitory effect of fludarabine on hepatocyte DNA synthesis (Fig.3b-c). However, BrdU incorporation following fludarabine removal was significantly greater than during drug treatment, suggesting BrdU positive hepatocytes progressed through S phase after drug washout (Fig.3b-c). Together, this data indicated that fludarabine treatment showed a transient and substantial inhibition of cell proliferation/DNA synthesis in mouse livers. Thus, increased proliferation in the liver was not the cause of increased gene targeting with fludarabine treatment.

To further study the relationship between cell proliferation and HR, we injected the rAAV8-Alb-P2A-GFP vector simultaneously with a week of BrdU, then co-stained hepatocytes which underwent HR (GFP signal) and DNA synthesis (BrdU) (Fig.3d). As before, fludarabine significantly increased GFP+ cells by ~5.4-fold (Fig.3e-f). qPCR analysis determined that on-target fusion GFP mRNA showed 6 to 7-fold greater levels in fludarabine versus PBS-treated animals (Fig.3g). Albumin mRNA expression remained unchanged by fludarabine treatment (Fig.3h).

We then examined whether GFP+ cells had progressed through S-phase as determined by BrdU incorporation. Surprisingly, we found BrdU (S-phase marker) colocalization with GFP (HR marker) positive cells was infrequent at 4.0% of all GFP+ cells in PBS-treated mice and 1.76% in the fludarabine-treated mice (Fig.3i). Thus, most GFP+ cells had not progressed through S-phase of the cell cycle during the timeframe of the experiment, regardless of drug treatment. Overall, progression through S-phase may not be a primary determinant of rAAV-HR *in vivo,* as only a small fraction of GFP+ cells had undergone DNA synthesis in the examined timeframe.

Fludarabine induced a transient DNA damage response

There are several different effects of fludarabine on cells: the drug is incorporated into DNA during replication or DNA repair[25–27], it causes the reduction of the dNTP pool by RNR inhibition, and causes premature transcription termination by incorporation into transcribing mRNA[27–29]. Any of these events can trigger DNA repair pathways, which can be linked to increased HR efficiency[30–32]. To assay for DNA damage response, we stained for phosphorylated Ser139 H2AX (γH2AX) in liver sections from the mice studied in Fig.3a after fludarabine treatment[33]. Minimal levels of γH2AX were detected in untreated or BrdU-only treated livers (Fig.4a-b). Mice treated with diethylnitrosamine (DEN), a potent mutagen, showed intense staining (Extended Fig.12c-d)[34]. During fludarabine treatment, mouse livers possessed widespread pan-nuclear γH2AX foci (Fig.4a-b). The number of positive nuclei lessened in the three days after fludarabine removal (Fig.4a-b). Western blotting for γH2AX using liver lysates from the same animals displayed similar tendencies to the immunohistochemical staining data (Fig.4c). We also found both siRNA-mediated knockdown of RRM1 as well as fludarabine treatment strongly increased γH2AX levels in Huh7 cells (Extended Fig.13). These results showed that fludarabine induced temporary DNA repair signaling in mouse liver, which may at least in part explain the mechanism of increased gene targeting efficiency with fludarabine.

Enhancement of gene targeting is not specific to all genotoxic treatments

Genotoxic treatments which induce DNA damage response can increase gene targeting rates in cultured cells[35] (Extended Fig.1b). To determine if genotoxicity is also a governing principle for rAAV gene targeting *in vivo*, we utilized DEN and Alb-P2A-hF9 co-injections in mice. DEN administration decreased body weight compared to controls in a dose-dependent manner (Extended Fig.14a). The highest dose of DEN (30 mg/kg) significantly increased hF9 plasma levels (about 3.6-fold) (Extended Fig.14b), whereas a low dose (10 mg/kg) did not significantly change hF9 levels. hF9 mRNA expression was increased by DEN administration (2- and 3.9-fold at low and high dose, respectively), whereas albumin mRNA expression was unchanged (Extended Fig.14c-d). On-target HR-derived fusion hF9 mRNA showed ~2-fold increase in DEN treated mice (Extended Fig.14e). These data suggested that some enhancement of hF9 expression was possible with DEN, however, DEN administration resulted in more severe toxicity, which was not observed in fludarabine-treated mice.

Fludarabine increased efficiency of CRISPR/Cas9-mediated gene editing

The induction of specific double-stranded breaks generated by programmable nucleases, such as CRISPR/Cas9 can increase rAAV-HR efficiency, which has been extensively investigated as promising gene editing therapies both *in vivo* and *ex vivo*[20,36]. To investigate whether CRISPR/Cas9-mediated HR is also affected by fludarabine, mice were injected with two rAAVs: one delivering saCas9 and a gRNA targeting the intron downstream of exon 14 in mouse *albumin* (AAV-Cas9) and one encoding a promoterless GFP sequence flanked by albumin homology arms (AAV-GFP-HDR) (Fig.5a). We examined various ratios of AAV-Cas9 to AAV-GFP-HDR (1:1, 1:5, 1:10) co-injections, with or without fludarabine. In all ratios tested, we found fludarabine treatment increased the percentage of GFP+ hepatocytes compared to controls (Fig.5b-c). qPCR analysis of the on-target fusion mRNA also showed an increase of

2 to 3.6-fold with fludarabine treatment (Fig.5d). The number of viral genomes in liver tissues at the end of the two-week experiment showed no significant changes with fludarabine treatment (Extended Fig.15a-b). To determine if fludarabine affected indels present at the target site, we performed targeted deep sequencing analysis using mouse liver tissues injected with AAV-Cas9 alone. The number of alleles with indels showed 2 to 3-fold increase in fludarabine-treated mice (Fig.5e). Additionally, the distribution of the top 12 alleles containing indels determined that fludarabine treatment resulted in an absence of larger insertions, compared to control (Fig.5f). SaCas9 mRNA levels at the time of tissue collection were unchanged by fludarabine treatment (Extended Fig.15c). Together these results showed that fludarabine also enhances CRISPR/Cas9-mediated gene editing *in vivo*, likely through stimulation of DNA repair and/or altered repair characteristics at the target site.

Discussion

In this study, we determined RNR inhibitors are useful drugs to enhance AAV-HR efficiency. Previous literature has described several compounds to increase gene editing efficiencies, however these approaches were only validated in cultured cells, or limited *in vivo* context, such as correction of gene mutation[38-42]. Our data showed that a short-term treatment with fludarabine, an FDA-approved drug, significantly enhanced AAV-HR *in vivo* without causing overt toxicity. Importantly, analysis of the genomic integration site at the *Albumin* locus confirmed precise recombination with no unexpected mutations in fludarabine-treated mice. In addition, our data showed that fludarabine also enhances gene editing with nuclease-based systems such as CRISPR/Cas9, implicating the use of fludarabine to increase editing efficiencies across numerous contexts, editing technologies, and genomic targets.

Prior investigations into the mechanisms governing AAV-HR determined that key HR-pathway factors are required for rAAV-HR[42]. In this regard, canonical HR is predominantly active during S/G2 phase of cell cycle when homologous sister chromatids are available as a repair templates during DNA replication[22–24]. Contrary to this S-phase centric HR principle, our present data showed that ~96% of hepatocytes undergoing HR *in vivo* were not co-immunostained with BrdU implicating that S-phase progression may not be a major determinant factor in AAV-HR and may not be the cause of fludarabine's enhancing effect. In support of this finding, we have found similar rates of rAAV-mediated gene targeting in neonatal and adult mouse livers, as well as in livers undergoing regeneration[6] (and unpublished data). Our observation that AAV-HR occurred mostly in cells that did not progress through S phase is in stark contrast to previous studies in cell culture[43–45]. It should be noted most of *in vivo* hepatocytes are in G0, which is considerably different from cultured cells and could contribute to the discordance[46]. Recently, it was reported that AAV-HR in cardiomyocytes occurred independently of S phase entry, which is in line with our present data[47].

This lack of S phase progression in HR+ hepatocytes prompted the hypothesis that fludarabine may have effects on non-proliferating hepatocytes. Fludarabine inhibits the catalytic subunit of RNR complex, RRM1, which functions throughout the cell cycle[18]. Thus, fludarabine can also function in non-dividing

cells by antagonizing basal levels of DNA repair due to decreased intracellular dNTP pools from RRM1 inhibition[25]. This notion is supported by our observation that fludarabine altered the repair characteristics at the targeted locus in mice injected with AAV-Cas9. Moreover, fludarabine, as a purine analogue, is incorporated into replicating DNA but also into nascent RNA, leading to premature transcription termination[48]. Indeed, by examining γH2AX levels, we confirmed widespread activation of DNA repair signaling in fludarabine-treated mouse livers where most of hepatocytes are in G0-phase. gH2AX is a hallmark of various DNA repair pathways and facilitates the recruitment and accessibility of repair factors to damaged DNA, which could directly or indirectly promote HR[49,50]. Moreover, the induction of DNA repair signaling could titrate host DNA damage factors, which process rAAV genomes, away from incoming rAAV particles, influencing transduction and perhaps recombinogenic forms of rAAV [51]. Therefore, activation of DNA repair can, at least partially, explain how fludarabine increased the probability of AAV-HR to occur in BrdU negative hepatocytes. In addition, given that DEN, a potent mutagen, induced higher levels of γH2AX, yet mediated a lesser enhancement of HR than fludarabine, it is unclear if DNA damage is required for AAV-HR. More likely is that the type of DNA damage and magnitude, in addition to other factors, may be important determinants for AAV-HR efficiency. Since the precise mechanism of rAAV-mediated gene targeting is not fully understood, particularly *in vivo*, unveiling the details of such mechanisms will be the focus of our future studies.

Overall, these novel discoveries show that a transient treatment fludarabine can safely enhance rAAV gene targeting efficacy, in a clinically relevant manner. Advanced approaches building upon this work will expand the utility of various gene editing technologies and permit lifelong therapeutic gene modification after a single administration of rAAV gene targeting vectors.

Methods

Cell culture and compound treatment

Huh7 cells and Hepa1-6 cells were purchased from JCRB and ATCC, respectively and were cultured in DMEM with 10% FBS, 2 mM glutamine. For hydroxyurea (Sigma), fludarabine (Fisher scientific), triapine (Fisher scientific) and Gallium (III) nitrate hydrate (Fisher scientific), cells were pretreated with each compound for 16 hours at indicated concentration and the cultured medium were replaced with fresh medium without compounds before rAAV transduction. For Torin-1, FK228 (Fisher scientific) (Fisher scientific), Trichostatin A, MG132 (Sigma) and Teniposide (Abcam), cells were treated with each compound for 24 hours at indicated concentration and rAAV was transduced 1 hour after compound addition.

Vectors

The AAV vectors containing ITR sequences used in this study are based on AAV type 2 backbone. CAG-Fluc, Albumin-P2A-hF9, HLP-hAAT vectors were prepared as described previously[52]. Albumin-P2A-GFP vector was generated by replacing hF9 coding sequence of the Albumin-P2A-hF9 vector with GFP coding

sequence using In-Fusion® HD Cloning Kit (TAKARA). SaCas9-sgRNA8 vector and Albumin-P2A-GFP vectors used for Figure.5 were prepared as described previously[20]. For construction of the GAPDH-P2A-GFP vector, human genomic GAPDH segments were PCR-amplified using Fw: 5'-GACTGTACAGGGCTGCTCACATATTCTGG-3' and Rv: 5'-CTGTGTACAGAGTGTATGTGGCTGTGGCCC -3' (both containing BsRG1 sites for cloning) and inserted between AAV2 ITRs into BsrGI restriction sites in a modified pTRUF backbone[53]. The genomic segment spans approximately 1.7 Kb upstream and 1.7 kb downstream to the GAPDH stop codon. We then synthesized a 1,359 bp fragment spanning the region at the end of the GAPDH locus between the two SexA1 sites to be cloned in the vector. In this fragment, the GAPDH stop codon was removed and it was inserted an optimized P2A coding sequence preceded by a linker coding sequence (glycine-serine-glycine) and followed by the GFP sequence (without the start codon). For Apoe-P2A-hF9 vector construction, a genomic fragment containing sequences used for both homology arms was amplified from mouse genomic DNA. Primers (5'- TCC ACA CCT GCC TAG TCT CG -3') and (5'- GTG CCA GAG GCA GTT GAG TT -3') were used to amplify a 2.9kb fragment and the PCR product was directly cloned into the pCR Blunt II TOPO vector using the Zero Blunt TOPO PCR cloning kit (Invitrogen), sequence verified. The left homology arm was amplified from the cloned ApoE genomic fragment using primers (5'- ata tca tcg atc gcg atg cat taa tta agc ggc cgA AGA CTG TAG GTC CTG ACC C –3') and (5'- ggt ggc gcc gct tcc TTG ATT CTC CTG GGC CAC -3'), the middle part containing hF9 sequence was amplified from Albumin vector using primers (5'- gcc cag gag aat caa GGA AGC GGC GCC ACC AAT -3') and (5'- gga gaa gga tac tca TGT CAG CTT GGT CTT TTC TTT GAT CC -3'), the right homology arm was amplified from the cloned ApoE genomic fragment using primers (5'- aag acc aag ctg aca TGA GTA TCC TTC TCC TGT CCT GC -3') and (5'- acg taa cag atc tga tat cac gcg tgt aca cta gtG CCC TGC TGA GTC CCT GAG -3'). Lower case letters indicate the overlapping sequences. Phusion Hot Start Flex (NEB) was used for all amplifications. Amplicons were assembled using the NEBuilder HiFi DNA Assembly Master Mix (NEB) according to instructions.

Animals

All animal works were performed in accordance to the guidelines for animal care at Stanford University or approved by the ICGEB review board, with full respect to the EU Directive 2010/63/EU for animal experimentation, and by the Italian Health Minister (authorization 996/2017-PR). Wild-type C57BL/6 (B6) mice were purchased from Jackson Laboratory (Bar Harbor, ME). We used 3-4-week-old juvenile mice to test the effect RNR small molecule inhibitors on gene targeting efficiency, as they are still undergoing development and growth, including in the liver.

Mouse AAV injection, drug dosing, bleeding and tissue sampling

B6 mice received tail vain injections of rAAV8 packaging each vector at the designated dose and were bled at indicated time points. Body weight of mice was measured using Scout pro portable scale (Ohaus) at indicated time points. Serum samples were obtained by centrifugation at 10,000 rpm for 10 minutes and used for ELISA assay of hF9 or hAAT, ALT enzyme measurements, and complete blood count tests. HU and fludarabine were resuspended in PBS and injected intraperitoneally with indicated dose/regimen.

For our studies examining the *in vivo* effects of RNR inhibitors, we chose to use HU and fludarabine due to their FDA approval and well-established safety profiles. The drug dosing was based on information from several preclinical studies.

Briefly, an initial dose of 1000 mg/kg injection of HU showed severe toxicity, leading us to reduce the dose to 300 mg/kg/day. For fludarabine, an LD_{10} for single or 5-daily IV infusions were about 980 and 400 mg/kg per dose, respectively, in male mice according to the product monograph of fludarabine. Additionally, five-day doses of ½ the LD_{10} or ~200mg/kg per dose was considered safe and administration of a smaller dose (125 mg/kg) three times a day over three days (1125 mg/kg total dose) produced the greatest activity in a leukemia tumor xenograft model. Using this information, we decided to use a dose of three 125 mg/kg injections per day (375 mg/kg/day) of fludarabine for 3 days. All drug administrations were through intraperitoneal injections (i.p.). For BrdU labeling of proliferating mice hepatocytes, BrdU was resuspended in PBS and intraperitoneally injected at 200 mg/kg per day for 3 days or 7 days. Diethylnitrosamine (DEN) solution was prepared using saline. We determined an appropriate dose of DEN after finding administration at 100 mg/kg resulted in severe weight loss requiring euthanasia. Dosing at 10 or 30 mg/kg as a single injection per day for 3 sequential days was well tolerated and used to examine this drug's genotoxic effect on gene targeting. At the end of each experiment, mice were anesthetized with isoflurane and perfused transcardially with PBS and then liver tissues were quickly harvested and cut into several pieces. The tissues for mRNA extractions were immediately submerged in RNAlater solution (Sigma) and stored at 4°C until use. For gDNA or protein extraction, tissues were snap-frozen in liquid nitrogen and stored at -80°C until use.

Hematology and liver pathology

CBC (complete blood count) and liver histopathological analysis were performed in mice injected with three 125 mg/kg injections of fludarabine per day, for 3 days. On the day of last injection and 4 weeks after that, mice were submitted to the Veterinary Service Center (VSC) at Stanford University for standard blood paneling tests and blinded analysis of liver pathology by a skilled veterinary pathologist.

AAV production

rAAV vectors were produced as previously described using a triple transfection protocol with Ca3(PO4)2 or PEI 25K, followed by purification by CsCl gradient[53] or using AAVpro® Purification Kit (All Serotypes) purchased from Takara Bio. Purified rAAVs were stored at -80°C until used. rAAV genomes were extracted and purified using QIAamp MinElute Virus Spin Kit (QIAGEN) and were titered by qPCR. The sequence information of primers are shown in Table1.

Firefly luciferase assay

Luciferase assays were performed using ONE-Glo™ Luciferase Assay System (Promega) following the manufacturer's instruction. Briefly, at indicated time points after rAAV (CAG-Fluc) transduction, the equal volume of the reconstituted substrate to the cultured medium was added to the cells grown in 96 well

plates and incubated for 10 minutes with gentle shaking. Luminescent activity was measured using a plate reader.

siRNA transfection

ON-TARGETplus siRNA against human RRM1 and POLR2A as well as scramble control siRNA were purchased from Dharmacon and were transfected into Huh7 cells using RNAiMAX (Life Technologies) according to the manufacturer's instructions. Final concentration of siRNA was 20 nM. AAVDJ packaging GAPDH-P2A-GFP vectors were added into the cultured medium at a multiplicity of infection (MOI) of 20,000 vector copies/cells at 48 hours after siRNA transfection. Flow cytometry was performed for detection of GFP positive fractions at the indicated time points.

Flow cytometry

Huh7 or Hepa1-6 cells were harvested and washed with cold PBS and resuspended in cold PBS containing 3% FBS. Cells were kept on ice and protected from light until analyzed. Singlet cells were determined based on FSC/SSC plot and GFP positive fractions were gated based on negative control which was non-transduced cells. The number of GFP expressing cells was evaluated using the BD FACSCalibur™ instrument and data were analyzed using the FlowJo software package.

RNA extraction and cDNA preparation

Total RNA was extracted using RNeasy micro plus kit (QIAGEN) according to the manufacture's protocol with DNase treatment. Liver tissue samples stabilized in RNA later solution (-100mg) were homogenized in RINO 1.5 mL Screw-Cap Tube filled with stainless steel beads and 600 mL of RLT buffer (including b-mercaptoethanol) using a bead homogenizer (Next Advance Bullet Blender Storm). Total RNA was extracted from the tissue lysates using RNeasy plus mini kit (QIAGEN) with additional on-column DNase treatment. cDNA was synthesized from 200-500 ng of total RNA using High-Capacity RNA-to-cDNA™ Kit (Life Technologies) according to the manufacturer's instructions.

gDNA extraction

Cultured cells were collected by trypsinization and washed with PBS. Total genomic DNA was extracted using QIAamp DNA Mini Kit (QIAGEN) according to the manufacture's protocol with RNase A treatment. Snap-frozen liver tissue (-100mg) were homogenized in RINO 1.5 mL Screw-Cap Tube filled with stainless steel beads and 600 mL of AL buffer using a bead homogenizer. Total RNA was extracted from the tissue lysates using DNeasy Blood & Tissue Kit (QIAGEN).

PCR and qRT-PCR

The polymerase chain reactions (PCRs) to amplify genomic regions where homologous integrations occurred (junction PCR) were performed using Q5® Hot Start High-Fidelity 2X Master Mix (New England Biolabs). The following cycling conditions were used: Human b-Actin (one cycle of 98°C for 30 sec, 28

cycles of 98°C for 10 sec, 60°C for 15 sec, and 72°C for 10 sec, and one cycle of 72°C for 2 min), GAPDH-P2A junction (one cycle of 98°C for 30 sec, 35 cycles of 98°C for 10 sec, 62°C for 15 sec, and 72°C for 1 min, and one cycle of 72°C for 2 min), Mouse albumin (one cycle of 98°C for 30 sec, 32 cycles of 98°C for 10 sec, 60°C for 10 sec, and 72°C for 2 min, and one cycle of 72°C for 2 min) , hF9-Albumin junction nested PCR (one cycle of 98°C for 30 sec, 20 cycles (1^{st} PCR) and 25 cycles (2^{nd} PCR) of 98°C for 10 sec, 62°C for 15 sec, and 72°C for 1 min, and one cycle of 72°C for 2 min). PCR products were analyzed in agarose gels containing Ethidium bromide and visualized using ChemiDoc Imaging Systems (Bio-Dad). Primer sequence information are listed in Table1.

Quantitative PCR was performed in duplicate using Apex qPCR GREEN Master Mix (Genesee Scientific) and CFX384 Touch Real-Time PCR Detection System (Bio-Rad) using the following cycling conditions: 95°C for 15 min, 45 cycles of 95°C for 10 sec, 60°C for 10 sec and 72°C for 10 sec, and one cycle of 95°C for 10 sec and 65°C for 1 min and 65-97°C (05°C/sec). Standard curves for each primer set were generated using serially diluted linearized plasmid and used for quantification. CFX Maestro Software was used for data analysis and relative mRNA expression levels were calculated by normalized against β-actin. All sequence information of primers is listed in Table1.

Protein extraction and western blotting

Total cell lysates from cultured cells or mouse liver tissues were prepared using RIPA buffer containing Halt™ Protease and Phosphatase Inhibitor Cocktail (both from Thermo Fisher). Liver tissues were homogenized in RINO 1.5 mL Screw-Cap Tube filled with stainless steel beads and 600 mL of RIPA buffer using a bead homogenizer. Protein concentration were measured using Pierce™ BCA Protein Assay Kit (Thermo Fisher) and the same amount of proteins for each sample were loaded into NuPAGE™ 4-12% Bis-Tris Protein Gels (Thermo Fisher). iBlot2 transfer system (Thermo Fisher) was used for western blotting. PVDF membranes were blocked with 5% BSA containing TBS-T buffer and the following 1^{st} antibodies were used. Anti-RRM1 (CST, 1:1000), HRP-conjugated anti-a-tubulin (CST, 1:2000) and anti-gH2AX (Novus Biologicals, 1:2000) antibodies. HRP-conjugated secondary antibodies were used, and signals were detected using Pierce™ ECL Plus Western Blotting Substrate (Thermo Fisher) and ChemiDoc Imaging Systems (Bio-Rad)

Southern blotting

Nuclear fractions of Huh7 cells were obtained using NE-PER™ Nuclear and Cytoplasmic Extraction Reagents (Thermo Fisher) and genomic DNA was extracted using QIAamp DNA Mini Kit (QIAGEN) and digested overnight with XhoI (New England Biolabs) to cut only host genomic DNA. Digested DNA was run in a 1% TAE agarose gel at room temperature O/N. After the electrophoresis, the gel was washed with denaturing buffer (3 M NaCl, 400 mM NaOH) twice for 5 minutes and DNA was transferred to an Amersham Hybond-XL membrane using transfer buffer (3 M NaCl, 8 mM NaOH) O/N. Membrane was washed with 2xSSC buffer for 5 minutes and then blocked with UltraPure™ Salmon Sperm DNA (Thermo Fisher) in QuikHyb Hybridization Solution (Agilent Technologies) for 1 hour at 65°C. Probes for GFP (574

bp) were generated using gel-purified PCR amplicons containing GFP sequence and BcaBEST™ Labeling Kit (TAKARA) and [α-32P]-dCTP (PerkinElmer), then probe hybridization were performed O/N at 65°C with rotation. The membrane was washed with 2xSSC buffer and with 2xSSC containing 0.1% SDS buffer at 65°C. Signals were visualized using Personal Molecular Imager™ System (Bio-Rad).

Immunohistochemistry staining of liver sections

For all in situ hybridization and immunostaining experiments liver tissue was dissected into 2-3 mm pieces and fixed for 24 hours in 10% neutral buffered formalin (Sigma Aldrich, St. Louis, MO) at 4 ºC. Tissue was subsequently processed through 10%, 20%, and 30% sucrose solutions for 24 hours each, then frozen embedded into OCT media (Sakura Finetek USA, Torrance, CA) with liquid nitrogen and 2-Methylbutane (Sigma Aldrich). Frozen tissue was sectioned into 16 µm thick sections using a Microm HM550 Microtome (Thermo Scientific, Waltham MA). Tissue sections were blocked with antibody diluent comprised of 5.0% normal donkey serum (Jackson Immuno Research, West Grove, PA) and 0.1% Triton-X 100 (Sigma Aldrich). GFP was stained with an anti-GFP chicken IgY primary antibody (Invitrogen, Carlsbad, CA) and phosphorylated Ser139 γH2AX was stained with a rabbit monocolonal (20E3) (Cell Signaling Technologies, Danvers, MA). Polyclonal secondary detection antibodies consisted of anti-chicken IgY antibody conjugated to Alexa Fluor 488 (Jackson Immuno Research) and polyclonal anti-rabbit IgG antibody conjugated to Alexa Fluor 594 (Thermo Scientific).

Detection of BrdU incorporated DNA was accomplished with heat denaturing in an antigen retrieval buffer (Advanced Cell Diagnostics, Newark, CA), followed by staining with a rat monoclonal anti-BrdU antibody (BU1/75 (ICR1)) (Abcam, Cambridge, UK) and secondary Alexa Fluor 594 antibody (Thermo Scientific). All IHC slides were mounted with Prolong Diamond Antifade with Dapi (Thermo Scientific) and imaged on a Zeiss LSM 880 confocal microscope. Specificity of all staining procedures was ensured with appropriate biological controls and control slides stained with secondary antibody only.

For eGFP experiments with Cas9 specimens were frozen in optimal cutting temperature compound (BioOptica, Milano, Italy) and 4 µm slices were obtained in a cryostat. Percentage of eGFP+ cells in liver specimens were detected by natural GFP fluorescence, while nuclei were visualized by Hoechst (10 lg/ml) staining. Slides were mounted in Mowiol 4-88 (Sigma). Images were acquired on a Nikon Eclipse E-800 epi-fluorescent microscope with a charge-coupled device camera (DMX 1200F; Nikon, Amstelveen, The Netherlands). Digital images were acquired on a Nikon Ti Eclipse inverted fluorescence microscope equipped with Intensilight Epi-fluorescence Illuminator, a Perfect Focus 3 system and 20× (NA 0.45) objective. Acquisition was performed with a DS-Qi2 16 Mpixel camera (Nikon). NIS Elements microscope imaging software (Nikon, version 4.6) was used to quantify the total number of cells (Hoechst staining) and the GFP positive cells. The settings of Automated Spot Detection were set in order to detect all bright spots with a typical minimum diameter of 8 µm. The function ”Detect all objects” was activated and spot detection-output were directly exported to Excel, where the data analysis was performed. For each animal an average 10000 nuclei were counted. Measurements (GFP+ cells/total nuclei) were averaged for each animal, and the results were expressed as mean ± SD for each treatment.

RNAScope *in situ* hybridization of hF9

Liver tissue was processed for RNA in situ hybridization as described above. Fixed frozen tissue was sectioned into 9 µm thick sections and RNAScope hybridization was performed according to the manufacturer's protocol (Advanced Cell Diagnostics). A custom probe was designed to detect codon-optimized human factor 9 mRNA, while control probes targeted either murine peptidylprolyl isomerase B (PPIB) (positive control for RNA quality) or bacterial 4-hydroxy-tetrahydrodipicolinate reductase (dapB) (negative control). RNA specificity was confirmed using RNase digestion of control tissue sections and slides were counterstained with 50% hematoxylin (Thermo Scientific). Imaging was performed using a Leica DM2000 brightfield microscope.

Image analysis

All image analysis was performed in a blinded manner. Analysis of BrdU incorporation was performed manually requiring nuclear colocalization of BrdU signal and greater signal intensity over background to be recorded as a positive nucleus. Signal from overtly non-hepatocyte nuclei directly associated with larger liver structures such as central veins or bile ducts were not included in tally. Analysis of BrdU incorporation and GFP colocalization was performed similarly. Scoring of phosphorylated Ser139 γH2AX was performed using ImageJ software.

Enzyme-linked immunosorbent assay (ELISA)

Mice serum samples were used to quantify hF9 or hATT protein expression levels. ELISA for hF9 was performed as previously described[6] with the following antibodies: mouse anti-hF9 IgG primary antibody at 1:1,000 (Sigma Cat#F2645), and polyclonal goat anti-hF9 peroxidase-conjugated IgG secondary antibody at 1:4,000 (Enzyme Research Cat#GAFIX-APHRP). ELISA for hAAT was performed as previously described[52].

Targeted Illumina Deep Sequencing

Genomic DNA was extracted from liver tissue using phenol/chloroform extraction, following incubation with RNAseA and Proteinase K. Genomic DNA was submitted to the Genome Engineering and IPSC Center (GEiC) at Washington University in St. Louis for targeted deep sequencing of the gRNA target site.

Statistics

GraphPad Prism was used for statistical analysis. Groups of two were analyzed by unpaired t test. More than two groups were compared by one-way ANOVA with Bonferroni correction. Statistical significance was assumed with P value <0.05 (*), <0.01(**) and <0.001 (***). Bars in graphs represent standard deviation for each group.

Image analysis was performed using two-tailed t-tests between groups. Normally distributed data, determined by D'Agostino Pearson test or Shapiro–Wilk test, was analyzed with parametric student's t

test if groups had equal variance. Groups with unequal variance were analyzed with an unpaired t test with Welch's correction. Significance in non-normally distributed data was determined using non-parametric Mann-Whitney U test.

Declarations

Tables 1-2 are not provided in this version of the manuscript.

Acknowledgments

This work was supported by grants from the NIH 2R01HL06427418A1, the Falk Medical Research Trust, NIH DK098132, and the National Hemophilia Foundation. A.F.M. was supported by intramural funds. The authors wish to acknowledge the Stanford Cell Sciences Imaging Facility (CSIF) for imaging analysis of liver sections, Stanford Genomics Facility for performing NGS and Stanford Veterinary Service Center (VSC) for animal health examinations. We also thank the Genome Engineering and IPSC Center (GEiC) at Washington University in St. Louis for performing NGS and analysis. The microscope was funded by the Stanford Beckman Center. The contents of this publication are solely the responsibility of the authors and do not necessarily represent the official views of the various funding bodies or universities involved.

Contributions

S.T. and M.A.K. designed the study. S.T., C.J.S and M.A.K. reviewed all data and wrote paper with all co-authors. S.T. performed *in vitro* studies. S.T., C.J.S. and F.Z. performed *in vivo* studies. C.J.S. performed imaging analysis. G.B. and A.F.M. performed *in vivo* study using CRISPR/Cas9 system. S.T., K.P. and G.A. designed and made plasmids. S.T. and K.P. performed rAAV production. H.J. performed ALT assay.

Data Availability Statement

The data generated in this manuscript are fully available upon reasonable request made to the corresponding author.

Corresponding author

Correspondence to Mark A. Kay

Declaration of Interests

S.T. and M.A.K. are named on patent applications related to this article. MAK has commercial affiliations and stock and/or equity in companies with technology broadly related to this article. S.T. is a current employee of Daiichi-Sankyo Co., Ltd. G.A. is a current employee of Sangamo Therapeutics.

References

1. Kotterman, M. A. & Schaffer, D. V. Engineering adeno-associated viruses for clinical gene therapy. doi:10.1038/nrg3742
2. Keeler, A. M. & Flotte, T. R. Recombinant Adeno-Associated Virus Gene Therapy in Light of Luxturna (and Zolgensma and Glybera): Where Are We, and How Did We Get Here? *Annu. Rev. Virol.* **6,** 601–621 (2019).
3. Wang, L., Wang, H., Bell, P., Mcmenamin, D. & Wilson, J. M. Brief Report Hepatic Gene Transfer in Neonatal Mice by Adeno-Associated Virus Serotype 8 Vector. doi:10.1089/hum.2011.183
4. Wang, L. *et al.* AAV8-mediated Hepatic Gene Transfer in Infant Rhesus Monkeys (Macaca mulatta). (2012). doi:10.1038/mt.2011.151
5. Cunningham, S. C., Dane, A. P., Spinoulas, A. & Alexander, I. E. Gene delivery to the juvenile mouse liver using AAV2/8 vectors. *Mol. Ther.* **16,** 1081–1088 (2008).
6. Barzel, A. *et al.* Promoterless gene targeting without nucleases ameliorates haemophilia B in mice. *Nature* **517,** 360–364 (2015).
7. Porro, F. *et al.* Promoterless gene targeting without nucleases rescues lethality of a Crigler-Najjar syndrome mouse model. *EMBO Mol. Med.* **9,** 1346–1355 (2017).
8. Hösel, M. *et al.* Autophagy determines efficiency of liver-directed gene therapy with adeno-associated viral vectors. *Hepatology* **66,** 252–265 (2017).
9. Schreiber, C. A. *et al.* An siRNA Screen Identifies the U2 snRNP Spliceosome as a Host Restriction Factor for Recombinant Adeno-associated Viruses. *PLOS Pathog.* **11,** e1005082 (2015).
10. Johnson, J. S. & Samulski, R. J. Enhancement of adeno-associated virus infection by mobilizing capsids into and out of the nucleolus. *J. Virol.* **83,** 2632–44 (2009).
11. Kia, A., Yata, T., Hajji, N. & Hajitou, A. Inhibition of histone deacetylation and DNA methylation improves gene expression mediated by the adeno-associated virus/phage in cancer cells. *Viruses* (2013). doi:10.3390/v5102561
12. Okada, T. *et al.* A histone deacetylase inhibitor enhances recombinant adeno-associated virus-mediated gene expression in tumor cells. *Mol. Ther.* (2006). doi:10.1016/j.ymthe.2005.11.010
13. Russell, D. W., Alexander, I. E., Dusty Miller, A. & Donnall Thomas, E. *Medical sciences DNA synthesis and topoisomerase inhibitors increase transduction by adeno-associated virus vectors Communicated by*. **92,** (1995).
14. Nicolson, S. C., Li, C., Hirsch, M. L., Setola, V. & Samulski, R. J. Identification and Validation of Small Molecules That Enhance Recombinant Adeno-associated Virus Transduction following High-Throughput Screens. *J. Virol.* **90,** 7019–7031 (2016).

15. Zhong, L. *et al.* Heat-shock treatment-mediated increase in transduction by recombinant adeno-associated virus 2 vectors is independent of the cellular heat-shock protein 90. *J. Biol. Chem.* **279,** 12714–23 (2004).
16. Marcus-Sekura, C. J. & Carter, B. J. *Chromatin-Like Structure of Adeno-Associated Virus DNA in Infected Cells*. *JOURNAL OF VIROLOGY* **48,** (1983).
17. Grimm, D. *et al.* In Vitro and In Vivo Gene Therapy Vector Evolution via Multispecies Interbreeding and Retargeting of Adeno-Associated Viruses. *J. Virol.* (2008). doi:10.1128/JVI.00254-08
18. Aye, Y., Li, M., Long, M. J. C. & Weiss, R. S. Ribonucleotide reductase and cancer: biological mechanisms and targeted therapies. *Oncogene* **34,** 2011–2021 (2015).
19. Marahatta, A., McElhinney, K., Howard, T. A. & Ware, R. E. Pharmacokinetics and Tissue Distribution of Hydroxyurea in a Mouse Model. *Blood* **126,** 4579–4579 (2015).
20. De Caneva, A. *et al.* Coupling AAV-mediated promoterless gene targeting to SaCas9 nuclease to efficiently correct liver metabolic diseases. (2019). doi:10.1172/jci.insight.128863
21. Maurer-Schultze, B., Siebert, M. & Bassukas, I. D. An in vivo study on the synchronizing effect of hydroxyurea. *Exp. Cell Res.* **174,** 230–243 (1988).
22. Wongt, E. A. & Capecchi, M. R. *NOTES Homologous Recombination between Coinjected DNA Sequences Peaks in Early to Mid-S Phase*. *MOLECULAR AND CELLULAR BIOLOGY* **7,** (1987).
23. Rothkamm, K., Krüger, I., Thompson, L. H., Löbrich, M. & Biophysik, F. Pathways of DNA Double-Strand Break Repair during the Mammalian Cell Cycle The induction and repair of individual IR-induced DSBs in * Corresponding author. Mailing address. *Mol. Cell. Biol.* **23,** 5706–5715 (2003).
24. Heyer, W.-D., Ehmsen, K. T. & Liu, J. Regulation of homologous recombination in eukaryotes. *Annu Rev Genet* **44,** 113–139 (2010).
25. Sandoval, A., Consoli, U., Plunkett, W. & Anderson, M. D. *Fludarabine-mediated Inhibition of Nucleotide Excision Repair Induces Apoptosis in Quiescent Human Lymphocytes1*. **2,** (1996).
26. Huang, P., Chubb, S. & Plunketts, W. *THE JOURNAL OF BIOLOGICAL CHEMISTRY Termination of DNA Synthesis by 9-&D-Arabinofuranosyl-Z-fluoroadenine A MECHANISM FOR CYTOTOXICITY**. **265,** (1990).
27. Huang, P., Sandoval, A., Van Den Neste, E., Keating, M. J. & Plunkett, W. *Inhibition of RNA transcription: a biochemical mechanism of action against chronic lymphocytic leukemia cells by fludarabine*. *Leukemia* **14,** (2000).
28. Pettitt, A. R. Mechanism of action of purine analogues in chronic lymphocytic leukaemia. *Br. J. Haematol.* **121,** 692–702 (2003).
29. Tseng, W. C., Derse, D., Cheng, Y. C., Brockman, R. W. & Bennett, L. L. In vitro biological activity of 9-beta-D-arabinofuranosyl-2-fluoroadenine and the biochemical actions of its triphosphate on DNA polymerases and ribonucleotide reductase from HeLa cells. *Mol. Pharmacol.* **21,** (1982).
30. Lans, H., Hoeijmakers, J. H. J., Vermeulen, W. & Marteijn, J. A. The DNA damage response to transcription stress. *Nature Reviews Molecular Cell Biology* **20,** 766–784 (2019).

31. Yasuhara, T. *et al.* Human Rad52 Promotes XPG-Mediated R-loop Processing to Initiate Transcription-Associated Homologous Recombination Repair. *Cell* **175,** 558–570.e11 (2018).
32. Stoimenov, I., Gottipati, P., Schultz, N. & Helleday, T. Transcription inhibition by 5,6-dichloro-1-beta-D-ribofuranosylbenzimidazole (DRB) causes DNA damage and triggers homologous recombination repair in mammalian cells. *Mutat. Res. Mol. Mech. Mutagen.* **706,** 1–6 (2011).
33. Stiff, T. *et al.* ATM and DNA-PK Function Redundantly to Phosphorylate H2AX after Exposure to Ionizing Radiation. *Cancer Res.* **64,** 2390–2396 (2004).
34. Den Engelse, L. & Philippus, E. J. In vivo repair of rat liver DNA damaged by dimethylnitrosamine or diethylnitrosamine. *Chem. Biol. Interact.* **19,** 111–124 (1977).
35. Ferrara, L., Parekh-Olmedo, H. & Kmiec, E. B. Enhanced oligonucleotide-directed gene targeting in mammalian cells following treatment with DNA damaging agents. *Exp. Cell Res.* **300,** 170–179 (2004).
36. Porteus, M. H., Cathomen, T., Weitzman, M. D. & Baltimore, D. Efficient Gene Targeting Mediated by Adeno-Associated Virus and DNA Double-Strand Breaks. *Mol. Cell. Biol.* **23,** 3558–3565 (2003).
37. Ferrara, L. & Kmiec, E. B. Camptothecin enhances the frequency of oligonucleotide-directed gene repair in mammalian cells by inducing DNA damage and activating homologous recombination. doi:10.1093/nar/gkh822
38. Paulk, N. K., Loza, L. M., Finegold, M. J. & Grompe, M. AAV-mediated gene targeting is significantly enhanced by transient inhibition of nonhomologous end joining or the proteasome in vivo. *Hum. Gene Ther.* **23,** 658–665 (2012).
39. Maruyama, T. *et al.* Inhibition of non-homologous end joining increases the efficiency of CRISPR/Cas9-mediated precise [TM: inserted] genome editing HHS Public Access Author manuscript. *Nat Biotechnol* **33,** 538–542 (2015).
40. Lin, S., Staahl, B. T., Alla, R. K. & Doudna, J. A. Enhanced homology-directed human genome engineering by controlled timing of CRISPR/Cas9 delivery. **3,** 4766 (2014).
41. Liu, M. *et al.* Methodologies for improving HDR efficiency. *Frontiers in Genetics* **10,** (2019).
42. Vasileva, A., Linden, R. M. & Jessberger, R. Homologous recombination is required for AAV-mediated gene targeting. *Nucleic Acids Res.* **34,** 3345–3360 (2006).
43. Liu, X. *et al.* Targeted Correction of Single-Base-Pair Mutations with Adeno-Associated Virus Vectors under Nonselective Conditions. *J. Virol.* **78,** 4165–4175 (2004).
44. Trobridge, G., Hirata, R. K. & Russell, D. W. Gene Targeting by Adeno-Associated Virus Vectors Is Cell-Cycle Dependent. *Hum. Gene Ther.* **16,** 522–526 (2005).
45. Vasileva, A. & Jessberger, R. Precise hit: Adeno-associated virus in gene targeting. *Nature Reviews Microbiology* **3,** 837–847 (2005).
46. Furchtgott, L. A., Chow, C. C. & Periwal, V. A Model of Liver Regeneration. doi:10.1016/j.bpj.2009.01.061

47. Kohama, Y. *et al.* Adeno-associated virus-mediated gene delivery promotes S-phase entry-independent precise targeted integration in cardiomyocytes. *Sci. Rep.* **10,** 1–13 (2020).
48. Huang, P. & Plunkett, W. Action of 9-beta-D-arabinofuranosyl-2-fluoroadenine on RNA metabolism. *Mol. Pharmacol.* **39,** (1991).
49. Mailand, N. *et al.* RNF8 Ubiquitylates Histones at DNA Double-Strand Breaks and Promotes Assembly of Repair Proteins. *Cell* **131,** 887–900 (2007).
50. Ji, J. H. *et al.* De novo phosphorylation of H2AX by WSTF regulates transcription-coupled homologous recombination repair. *Nucleic Acids Res.* **47,** 6299–6314 (2019).
51. Mano, M., Ippodrino, R., Zentilin, L., Zacchigna, S. & Giacca, M. Genome-wide RNAi screening identifies host restriction factors critical for in vivo AAV transduction. *Proc. Natl. Acad. Sci.* (2015). doi:10.1073/pnas.1503607112
52. Lu, J. *et al.* A 5¢ Noncoding Exon Containing Engineered Intron Enhances Transgene Expression from Recombinant AAV Vectors in vivo. doi:10.1089/hum.2016.140
53. Grimm, D., Pandey, K., Nakai, H., Storm, T. A. & Kay, M. A. Liver Transduction with Recombinant Adeno-Associated Virus Is Primarily Restricted by Capsid Serotype Not Vector Genotype. *J. Virol.* **80,** 426–439 (2006).

Figures

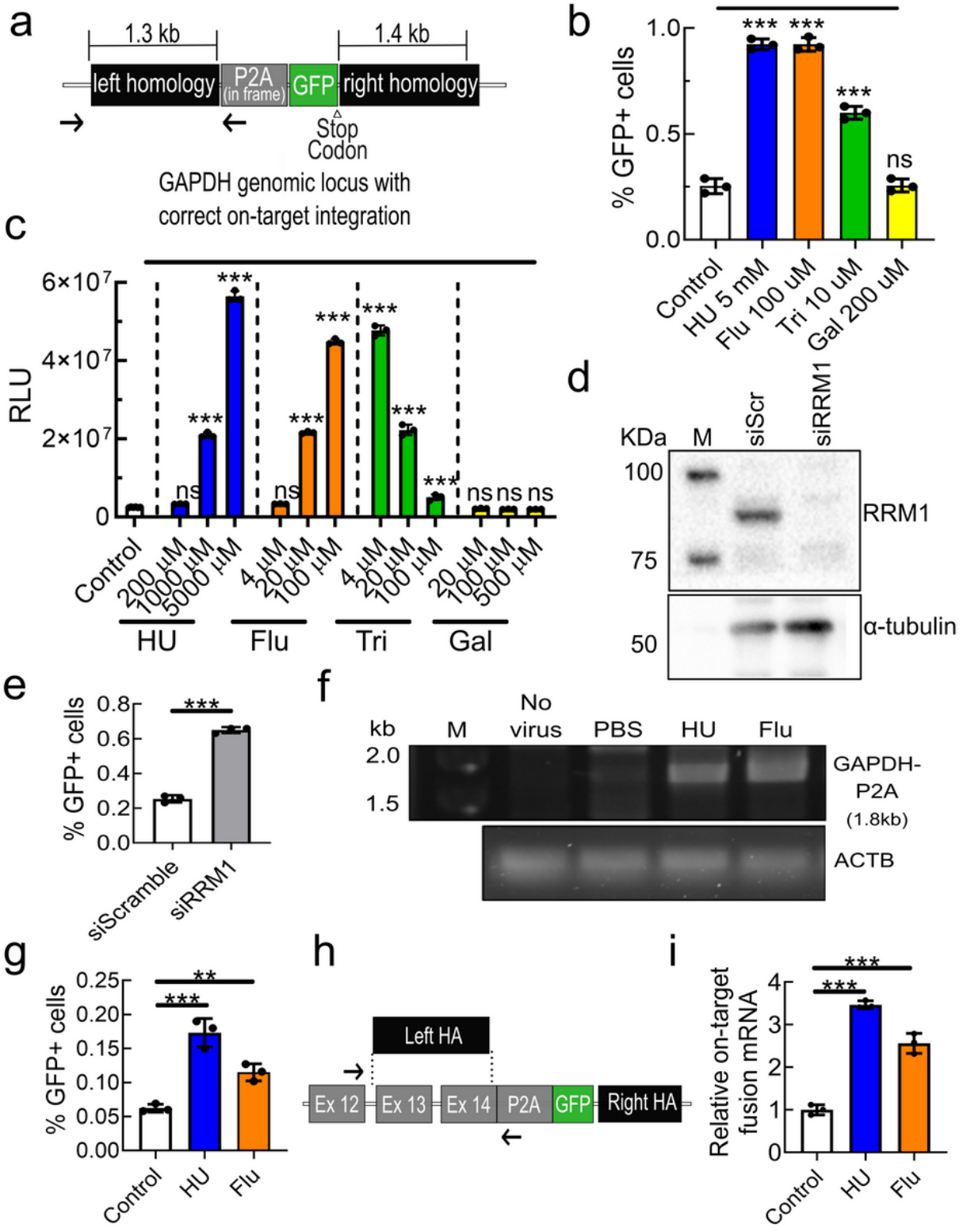

Figure 1

Inhibition of ribonuclease reductase increased the efficiency of gene targeting in human and mouse cell lines a, Schematic of the GAPDH genomic locus after on-target homologous recombination with the GAPDH-P2A-GFP gene targeting vector. The positions of in and out PCR primers, to detect site-specific integration, are indicated by black arrows. b, Huh7 cells were treated with RNR inhibitors and transduced with an AAVDJ gene targeting vector GAPDH-P2A-GFP. Flow cytometry analysis of GFP positive fractions

was performed at 14 days after AAV transduction. HU, hydroxyurea. Flu, fludarabine. Tri, Triapine. Gal, Gallium nitrate. Error bars represent s.d.; n=3. c, Huh7 cells were treated with RNR inhibitors and transduced with an AAVDJ vector expressing Fluc from the CAG promoter. Luciferase activity was measured 24 hours later. RLU, relative light unit. Error bars represent s.d.; n=3. d and e, Huh7 cells were transfected with RRM1 siRNA, then transduced with the GAPDH-P2A-GFP vector. d, Western blotting was performed 2 days after transfection to assess the knockdown of RRM1. e, GFP positive fraction was analyzed by flow cytometry 3 days after transduction. Error bars represent s.d.; n=3. Significance was determined using a two-tailed t test. f, A semi-quantitative PCR to detect accurate on-target integration at the GAPDH locus. Genomic DNA was extracted from Huh7 cells treated with indicated RNR inhibitors, 14 days after AAV transduction. Amplification of the ACTB locus was used as a control. h, Schematic of the mouse albumin locus after homologous recombination with gene targeting Albumin-P2A-GFP vector. The positions of qPCR primers to detect on-target integrated fusion mRNA are indicated. g, Murine Hepa1-6 cells were treated with indicated RNR inhibitors and transduced with the AAVDJ packaged Alb-P2A-GFP targeting vector. Flow-cytometry analysis of GFP positive fractions at 14 days after AAV transduction is shown. Error bars represent s.d.; n=3. i, Total RNA was extracted from transduced Hepa1-6 cells and qPCR was performed to quantify expression levels of on-target integrated Alb-P2A-GFP fusion mRNA. Actb mRNA was used for normalization and data shown as relative expression to control. Error bars represent s.d.; n=3. Significance was determined using one-way ANOVA analysis with Dunnett's test for multiple comparisons for all data in this figure, unless otherwise indicated. A single asterisk (*) represents a p-value of <0.05, ** is <.01, and *** is <.001; ns is not significant.

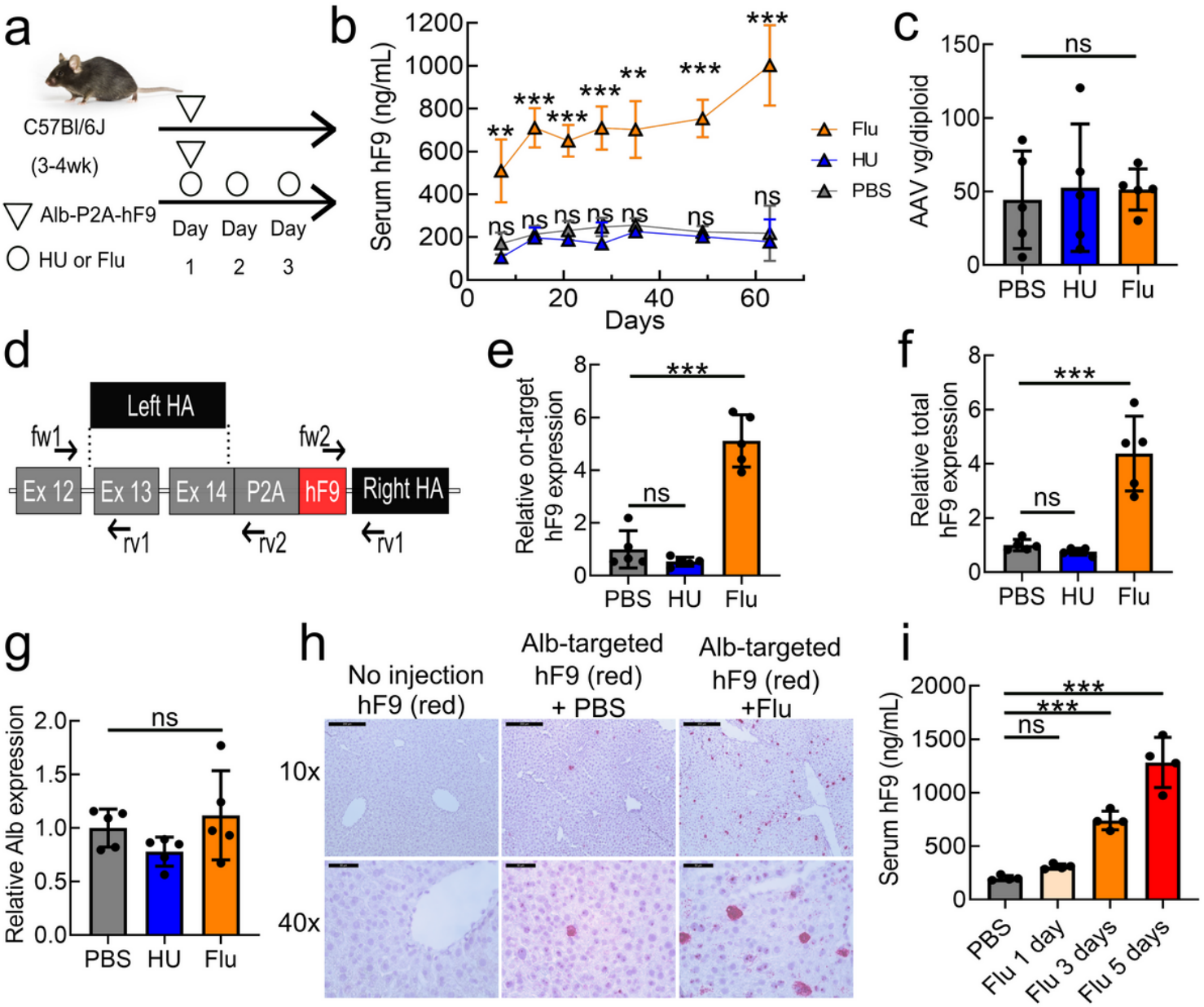

Figure 2

Fludarabine administration increased the efficiency of gene targeting in hepatocytes of mice a, The in vivo experimental design consisted of HU (300 mg/kg) once per day or Flu (125 mg/kg) i.p. injections three times per day through Day 1 to Day 3. Mice were also injected i.v. with the rAAV8 Alb-P2A-hF9 targeting vector (1.0x1011 vg/mouse) on Day 1, immediately after the second HU or Flu injection. Blood was collected at the indicated time points and mice were sacrificed on the last day of blood collection for liver tissue analyses. b, hF9 protein levels in mouse serum were determined using a sandwich ELISA, following gene targeting Alb-P2A-hF9 vector injection, with or without drug treatment, over a 65-day period. Error bars represent s.d; n=5.Significance testing was performed by two-way ANOVA analysis. c, Genomic DNA was extracted from liver tissues 65 days after Alb-P2A-hF9 vector injection and qPCR was performed to quantify the amount of total AAV genomes. Actb primers were used for quantification of the number of diploid genomes. Error bars represent s.d.; n=5. d, A schematic representing the mouse

albumin locus after homologous recombination with gene targeting Alb-P2A-hF9 vector. Exon-intron structure and the positions of qPCR primer pairs used for e-h are indicated. e-g, Total RNA was extracted from the mouse liver tissues in Fig2b. qPCRs were performed to quantify the expression levels of on-target integration-derived Alb-P2A-hF9 fusion mRNA (primers Fw1 and Rv2, black arrows) (e), total hF9 mRNA (Fw2 and Rv3) (f), and endogenous albumin mRNA (Fw1 and Rv1) (g). Actb mRNA was used for normalization and data is shown as relative expression to the PBS-treated group. Error bars represent s.d.; n=5. h, Detection of hF9 mRNA (red) in liver sections using RNAScope in situ hybridization. Liver sections of mice from non-injected, PBS-treated, and Flu-treated groups were used for hybridization and counterstained with hematoxylin. Representative images from each injected group are shown. i, The effect of different Flu dosing regimens on gene targeting efficiency. Flu (125 mg/kg) was administered i.p. three times per day for 1, 3, or 5 sequential days. Mice were i.v. injected at Day 1 with the Alb-P2A-hF9 targeting vector (1.0x1011 vg/mouse) , immediately after the second administration of Flu. Blood was collected 2 months after AAV injection and hF9 protein levels were determined via ELISA. Error bars represent s.d.; n=4 (hFIX serum levels throughout this time course data are provided in Extended Figure 6). Significance was determined using a one-way ANOVA analysis for all data in this figure unless otherwise indicated.

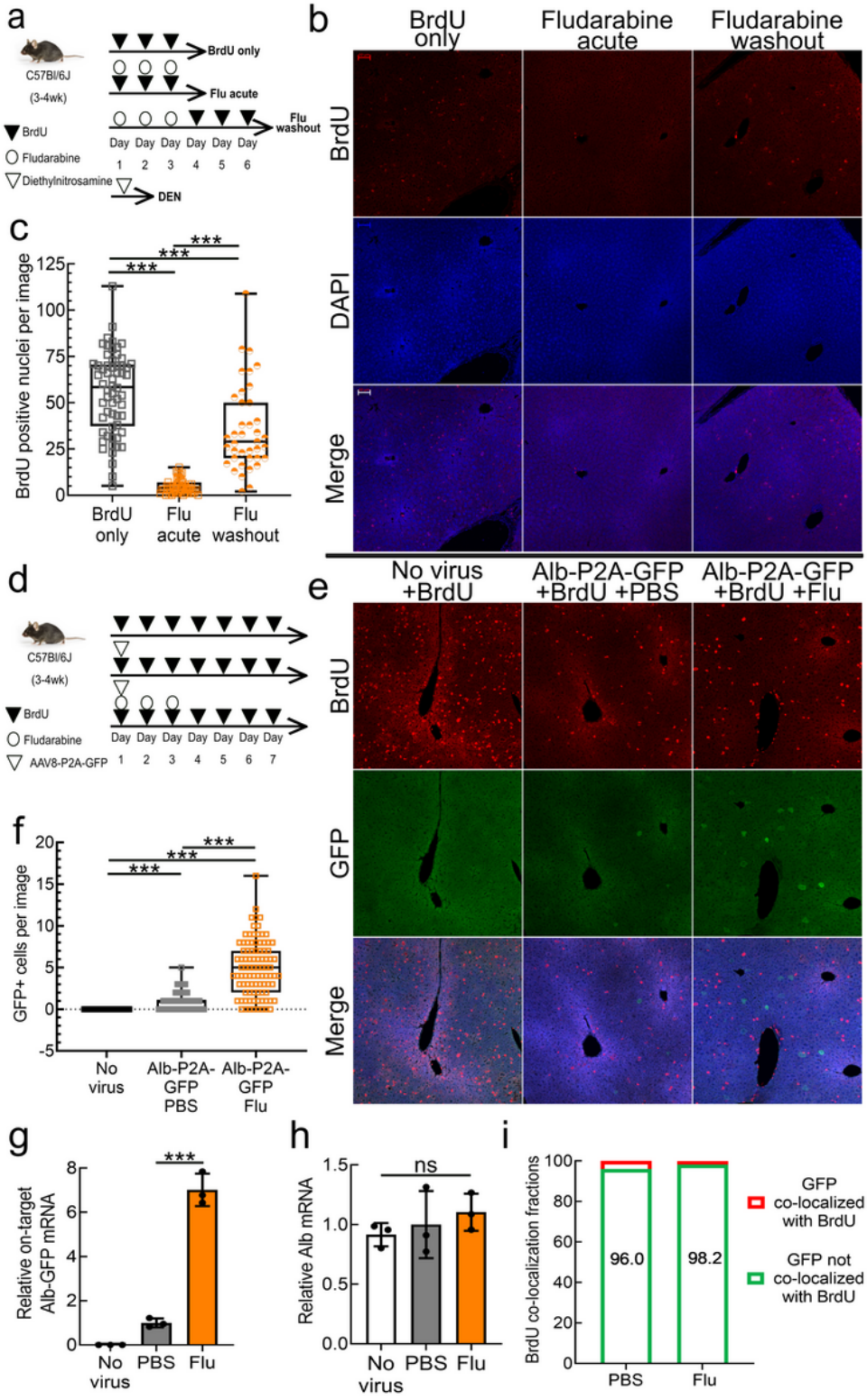

Figure 3

Fludarabine transiently inhibits S-phase progression and rAAV gene targeting occurs in hepatocytes that have not progressed through S-phase a, A schematic of injection schedules for assessing cell proliferation. Mice were i.p. injected with BrdU (200mg/kg) in PBS once per day for three days to label proliferating hepatocytes. Some mice were simultaneously injected with Flu (125 mg/kg, three times per day for three days), while the final group were treated with the same Flu injection schedule prior to the

three days of BrdU injection. n=3. b, Six hours after the last injection, mice were sacrificed and liver tissue sections were used for immune-staining using an anti-BrdU antibody. Representative images from each injected group are shown with BrdU labeled nuclei (red) and a DAPI counterstain (blue). All images were taken with 20x objective with identical exposure and settings. c, Images of BrdU labeled nuclei were quantified from each group and displayed as the number of BrdU+ nuclei per field of view. Images used for quantification are from two or more slides per animal, three animals per group, and two or more independent stains. Significance was determined using D'Agostino Pearson test for normality and non-parametric Mann-Whitney U test. Box and whisker plots show minimum to maximum values by bars, with the box representing the 25th to 75th quartiles and a median line. d, To label proliferating cells in the liver, mice were i.p. injected with BrdU once per day for seven days. On Day 1 of BrdU injections, two groups of mice were also injected with the gene targeting Alb-P2A-GFP vectors packaged in rAAV8. One of these groups was treated with Flu (125 mg/kg, three times per day) i.p. for the first three days of BrdU injection time course. e, On day 7, mice were sacrificed and liver tissue sections were used for IHC staining of BrdU (red) and GFP (green) with a DAPI nuclear stain (blue). Representative images from two mice per group are shown. f, GFP+ cells were quantified for all mice as the number of positive cells per 20x field of view. Significance was determined by Mann-Whitney U testing. Images used for quantification are from two or more slides per animal, with three animals per group. g-h, Total RNA was extracted from liver tissue. qPCR determined levels of on-target integration derived Alb-P2A-GFP mRNA and endogenous albumin mRNA, as described previously. i, The number of GFP+ cells that colocalized with BrdU (i.e. undergone S-phase DNA synthesis) were quantified and displayed as the percent of total GFP+ cells per group.

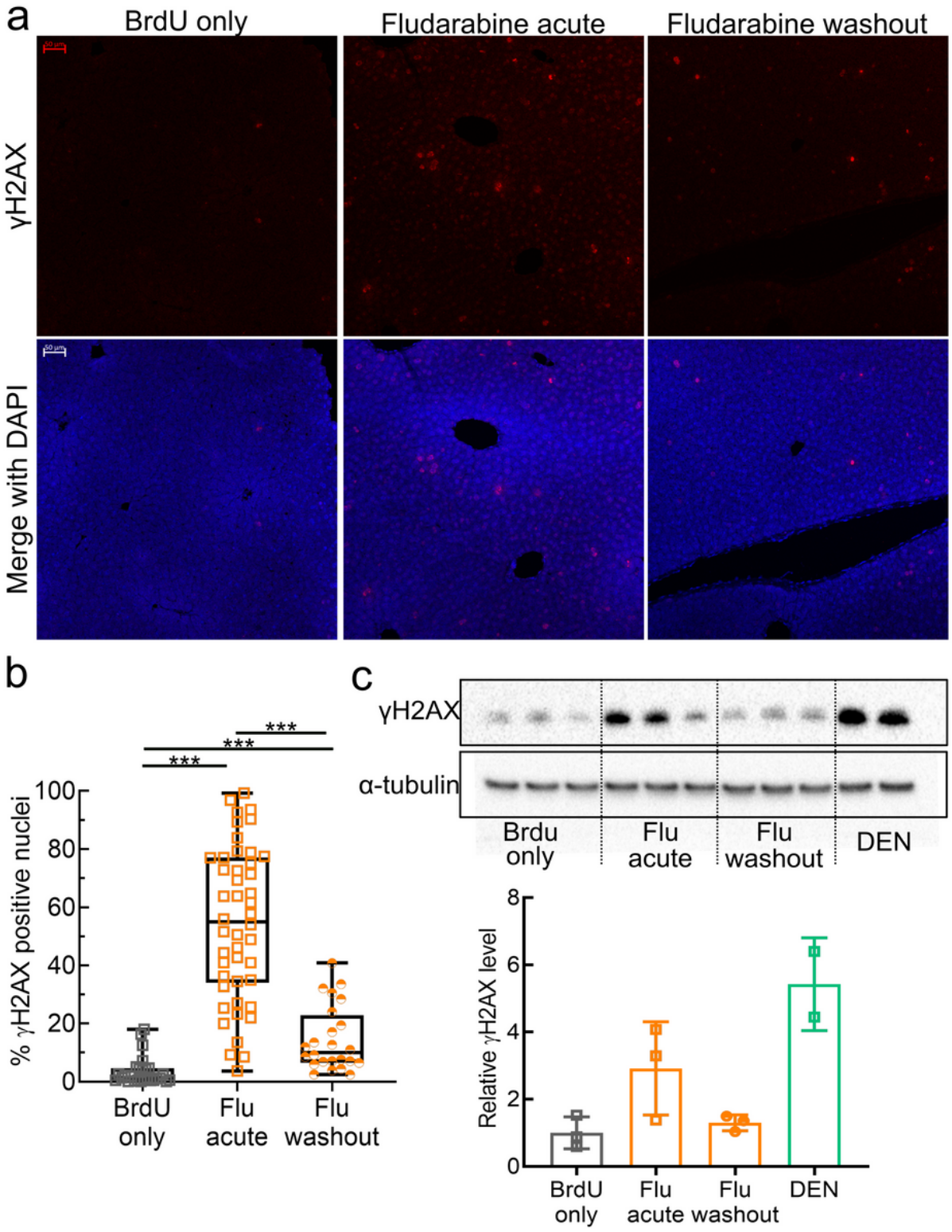

Figure 4

Fludarabine induces a transient DNA damage response in mice a, Liver tissue sections from the same animals in Fig3a-c were also stained for the DNA damage response marker phosphorylated Ser139 on H2AX (γH2AX). Representative images are shown with γH2AX (red) and DAPI (blue). b, Images of γH2AX nuclei were quantified from each group and displayed as the percentage of γH2AX+ nuclei out of all nuclei. Images used for quantification are from two or more slides per animal, three animals per group,

and two or more independent stains. Significance was determined using a D'Agostino Pearson Test for normality and a non-parametric Mann-Whitney U test or parametric Welch's T test. Box and whisker plots show minimum to maximum values by bars, with the box representing the 25th to 75th quartiles and a median line. c, Liver tissue lysates from the same mice were used for Western blotting of γH2AX, and α-tubulin as a loading control (top). Image analysis quantification of the γH2AX band intensity in the Western was normalized to α-tubulin (bottom). Each lane is data from one animal except for DEN-treatment, which is two lanes with a single mouse sample.

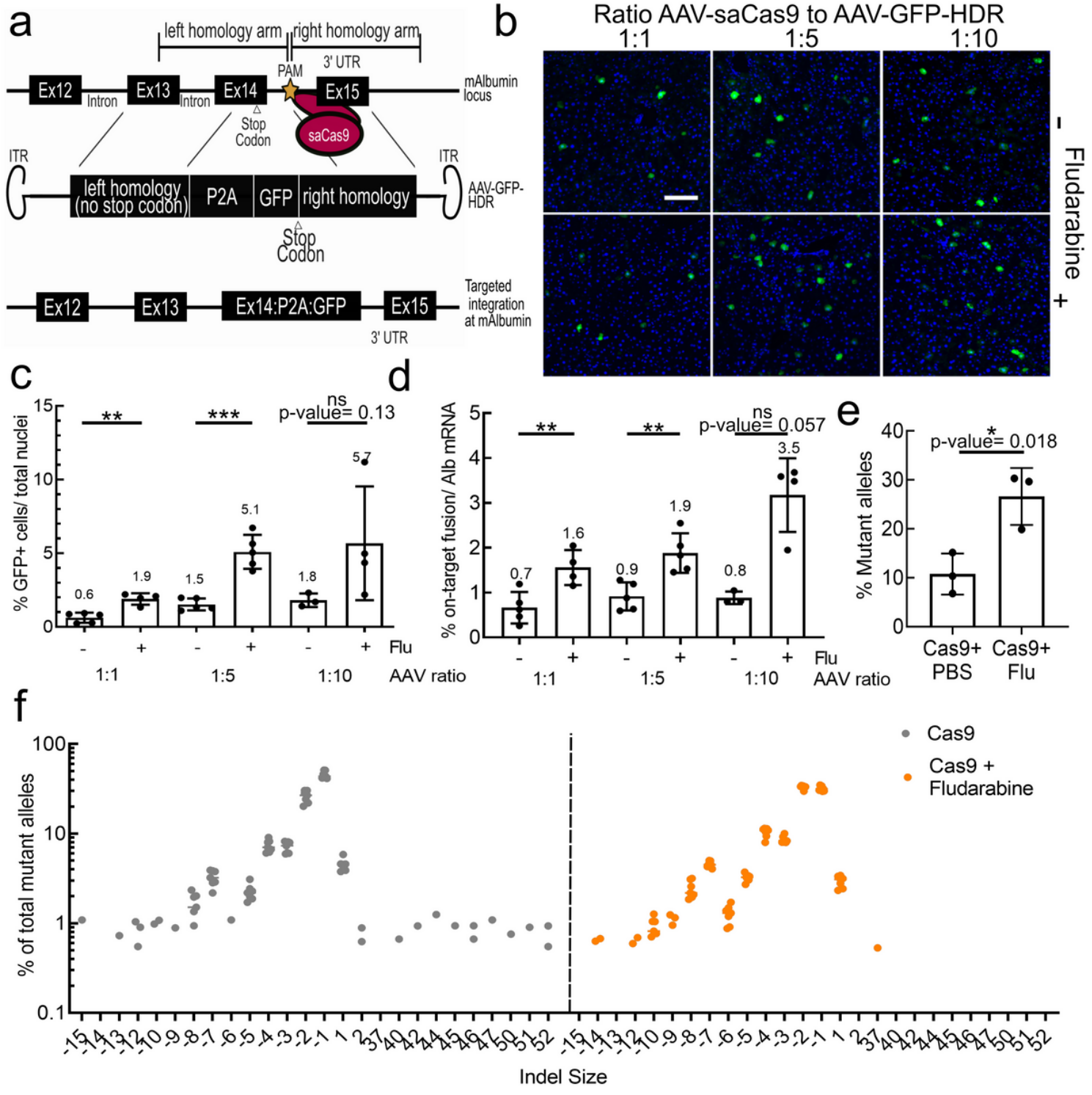

Figure 5

Fludarabine increases CRISPR/Cas9 gene editing efficiency in vivo. a, A schematic showing saCas9 targeted to the intron downstream of exon 14 in the mouse Albumin locus, delivered by AAV-saCas9. Homology-directed repair is accomplished using an AAV-encoded repair template, AAV-GFP-HDR, which contains a P2A-GFP transgene flanked by sequences homologous to the gRNA target site. The PAM site of the AAV-GFP-HDR was mutated to avoid self-targeting. b, Mice were treated with PBS or Fludarabine, as previously described, and co-injected with AAV-saCas9 and AAV-GFP-HDR. Three ratios of AAV-saCas9 to AAV-GFP-HDR vector were used (1:1, 1:5, and 1:10) with each part representing 6.0E12 vg/kg. Two weeks after injection with drug and vectors, mice were harvested and liver tissue sectioned for imaging of native GFP expression. Representative images of GFP positive cells are shown. n=3 to 5 animals per group. c, GFP+ cells were quantified from multiple images per animal and graphed. Significance testing was performed using two-tailed t tests including Welch's correction if data had unequal variance. Each dot represents data from an individual animal. d, Total RNA was extracted from liver tissue of all animals and used for quantification of the level of on-target HR-derived fusion mRNA or albumin mRNA by qPCR. mRNA levels were normalized to mActb mRNA. Data is displayed as a percentage of fusion mRNA out of all albumin mRNA. Each dot represents data from an individual animal. Significance testing was performed using a two-tailed t test or Mann-Whitney U test for non-normally distributed data. e, Separately, mice were injected with 6.0E12 vg/kg of AAV-saCas9, with or without fludarabine treatment. Genomic DNA was extracted from liver tissue two-weeks later and targeted deep sequencing of the gRNA target site was performed in replicate. Data is normalized to sequencing data from a non-injected control mouse and displayed as a percentage of alleles containing indels (insertion or deletions). n=3 mice per group. Significance testing was performed with a two-tailed t test. f, The top 12 mutant alleles from the targeted deep sequencing was analyzed for all animals and technical replicates. Indels were graphed as the percentage of reads from all mutant alleles based upon size (x-axis).

Supplementary Files

This is a list of supplementary files associated with this preprint. Click to download.

- ExtendedFiguresandlegends10312020.pdf